Structural and dynamical consequences of interactions in interfacial systems

Uzi Landman, W. D. Luedtke, and M. W. Ribarsky
School of Physics, Georgia Institute of Technology, Atlanta, Georgia 30332

(Received 31 March 1989; accepted 3 April 1989)

Basic understanding of the structure and dynamics of materials and their response to external perturbations requires knowledge on the microscopic level, of the underlying energetics and atomic dynamics, whose consequences we observe and measure. Coupled with the above is the everlasting quest to observe and understand natural phenomena on refined microscopic scales, which provides the impetus for the development of experimental and theoretical techniques for the interrogation of materials with refined spatial and temporal resolution. In this paper we review molecular dynamics simulations for studies of the energetics and dynamical response of materials to external mechanical perturbations. Applications to investigations of solid and liquid interfacial systems under stress and to studies of the consequences of tip–substrate interactions in atomic force microscopy are demonstrated.

I. INTRODUCTION

Basic understanding of the structure and dynamics of materials and their properties often requires knowledge on a microscopic level of the underlying energetics and interaction mechanisms whose consequences we observe and measure. The everlasting quest to observe and understand nature on microscopic scales[1] is a dominant trend in science, leading to the development of conceptual, technological, and experimental devices which allow interrogation of nature with refined spatial and temporal resolution. Elucidation of the structure, dynamics, mechanical properties, and response of material systems to external perturbations on the atomic level, are key issues in developing a fundamental understanding of varied systems and phenomena of coupled basic and technological interest, such as surface and interface systems, surface reactions and catalysis, electrochemical interfaces, understanding of structure–function relationships in biomolecular systems, microelectronics materials, tribology, lubrication, wear, material fatigue and yield, crack propagation, stress induced phase and structural transformations, and hydrodynamical phenomena in confined fluid systems, to name just a few. Although most of the above listed phenomena represent everyday experiences and have been observed and studied for a long time, detailed microscopic theories of them (with few exceptions) are lacking. Nevertheless large bodies of empirical data and in some cases phenomenological model descriptions have been developed.

On the experimental front the developments of the surface force apparatus (SFA)[2,3] scanning tunneling microscopy (STM)[4] and of the related atomic force microscopy (AFM)[5] broaden our perspectives and abilities to probe the morphological and electronic structure and the nature of interatomic forces in materials, open new avenues[6] for microscopic investigations and manipulations of technological systems and phenomena such as tribology,[3,7] lithography and in biochemical applications,[6] and present exciting possibilities for the development of miniaturized electronic, magnetic and optical devices.

In the latter two techniques a sharp tip is brought close to the surface and either the tunneling current (STM) or deflection of a flexible cantilever holding the tip (AFM) are monitored, either by tunneling or by optical interferometry as the surface is scanned. Since the proximity of the tip to the surface may induce structural modifications in both the substrate and the tip, the nature of the tip–substrate interactions and their consequences are key issues in the development of these spectroscopies (as is the issue of probe–system interaction in all methods of microscopic resolution). Of particular interest are questions related to the dynamical response of the substrate (and tip) which may result in temporary or permanent modifications of the local properties, and those related to the effect of system conditions (such as temperature) which may influence the response as well as affect the spatial resolution. It has been indeed suggested[8] that STM images can be dominated by elastic deformations induced by the tip–substrate interatomic forces and a transition from a tunnel regime to point contact has been observed.[9]

Recently, the AFM has been applied to study the topography and frictional forces at the atomic scale.[7] Furthermore, recent investigations[3] of the dynamical properties of molecularly thin liquid films confined between two surfaces, using an extension of the SFA, have demonstrated the direct consequences of microscopic molecular structure and interactions on the structural and dynamical properties of such sytems both under static and steady-state shear-flow conditions.

On the theoretical front computer molecular dynamics (MD) simulations[10–19], which are in a sense computer experiments where the evolution of a physical system is simulated, with refined temporal and spatial resolution, via a direct numerical solution of the model equations of motion, open new avenues in investigations of the microscopic origins of material phenomena. These methods alleviate certain of the major difficulties which hamper other theoretical approaches, particularly for complex systems such as those characterized by a large number of degrees of freedom, lack of symmetry, nonlinearities and complicated interactions. In

 0734-2101/89/042829-11$01.00

addition to comparisons with experimental data which provide guidance in the interpretation of data and the impetus for new measurements, computer simulations can be used as a source of physical information which may not be accessible to laboratory experiments, and in some instances the computer experiment itself serves as a testing ground for theoretical concepts.

In this paper we review recent molecular dynamics studies of systems and phenomena related to the rapidly evolving field of nanoscience. We address and demonstrate investigations of three issues: (i) the consequences of dynamical tip–substrate interactions, (ii) the nature of bounded thin fluid films in equilibrium and in steady-state flow under shear, and (iii) the microscopic energetics, dynamics and response of interfacial systems to external perturbations.

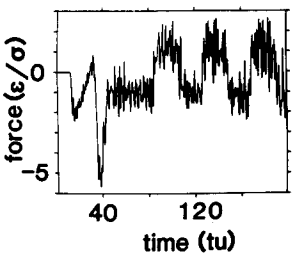

FIG. 1. Total F_z force (in units of 1.6572×10^{-9} N) on the small rigid silicon tip as it is lowered to a distance of 1.227 Å, equilibrated and scans along the surface. Time is in units of tu $= 7.6634\times10^{-14}$ s. Note the sharp variation in the force as the tip is lowered and the periodic oscillations reflecting the atomic structure of the surface during the scan ($t\gtrsim60$).

II. CONSEQUENCES OF TIP–SUBSTRATE INTERACTIONS

To investigate the consequences of the dynamical interactions between the tip and the substrate in AFM we have performed MD simulations, employing the Stillinger–Weber (SW) potentials for silicon[20] which include two- and three-body interactions and which have been used recently in a number of investigations of bulk, surface and interface properties of this material.[17–24] Since both the substrate and tip consist of the same material, these simulations correspond to the case of a reactive tip–substrate system. Our simulations,[17–19,23] in both the constant-tip-height and constant-force scan modes, reveal that the *local* structure of the surface can be stressed and modified as a consequence of the tip–substrate dynamical interaction, even at tip–substrate separations which correspond to weak interaction. For large separations these perturbations anneal upon advancement of the tip while permanent damage can occur for smaller separations. For the material that we simulated (Si), we do not find long-range elastic deformations, which may occur in other circumstances[8] depending upon the elastic properties of the material and the nature of interactions. Furthermore, we find that the characteristics of the data depend upon the geometry of the scan, the degree of perfection of the substrate and the temperature. We identify various dynamical events including stick–slip phenomena, which could be experimentally resolved, using current estimates,[5,6] and which would influence the analysis of data, as well as pointing to ways in which the tip could be used for atomic scale manipulations of the material.

In our simulations the system consists of N_L layers of dynamic Si particles with n_L atoms per layer, exposing the (111) surface, and interacting with two layers of a static Si substrate of the same structure. In simulations involving a small tip $N_L = 4$ and $n_L = 49$, while in simulations involving larger tips $N_L = 6$ and $n_L = 100$. The two-dimensional calculational cell, defined by the $(1\bar{1}0)$ and $(10\bar{1})$ vectors, is periodically repeated parallel to the (111) plane. Two types of tips were employed in our simulations. First, we have used a sharp tip simulated by four Si atoms in an initial tetrahedral configuration, "mounted" on and interacting with two layers of silicon atoms which serve as a holder. In addition we have employed larger tips consisting of 102 atoms, which were either ordered [exposing a 16 atoms (111) planar facet] or disordered. The equations of motion, governed by the SW potential,[20] are integrated using a fifth-order predictor–corrector algorithm with a time step $\Delta t = 1.15\times10^{-3}$ ps, [or 0.015 time units (tu) where tu $= 7.6634\times10^{-14}$ s]. Throughout we use $\epsilon = 50$ kcal/mol as the unit of energy, $\sigma = 2.0951$ Å as the unit of length, and $\epsilon/\sigma = 1.65728\times10^{-9}$ N as the unit of force. The kinetic temperature is controlled to room temperature via scaling of particle velocities in the bottom layer of the dynamic substrate. Both constant-tip-height and constant-force scan modes were simulated.

First we investigate the process of lowering a tip towards the substrate which is then followed by either raising of the tip or scanning laterally across the surface in either a constant height or constant-force mode. The total force in the normal (z) direction on a rigid four-atom tip (arranged as a tetrahedron) is shown in Fig. 1. Starting with the system at equilibrium and outside the range of interaction with the substrate [see snapshot of the system initial configuration in Fig. 2(a)] the tip is lowered slowly toward the surface. Initially the tip experiences an attractive force ($F<0$) accompanied by a lifting of the surface atom right below the lowermost tip atom, as seen in the snapshot given in Fig. 2(b). As the tip approaches the surface the attraction diminishes culminating in a repulsion ($F_z>0$ at ~30 tu in Fig. 1) which turns into an attraction in a sudden manner (see Fig. 1 at $\lesssim40$ tu). Inspection of the real space trajectory of the system reveals that these events are associated with a formation of an interstitial defect where the surface atom is pushed into the interstitial position in the second layer. Further relaxation of the system at tip-to-substrate separation of 1.227 Å (corresponding to a *repulsive* region of the interatomic potential) results in a *net attractive* force caused by the *tip-induced local reconstruction* [see Fig. 2(c)]. At this point the latteral scan begins (in the $[1\bar{1}0]$ direction) at a rate which assures tip–substrate relaxed configurations throughout the scan. As the tip scans (at constant height) over the surface the recorded normal force on it oscillates with the periodicity of the substrate, being repulsive ($F_z>0$) when the tip traverses the region between atoms and attractive over the substrate atoms (Fig. 1, $t\gtrsim60$ tu). Snapshots of the system at different tip locations (starting from the tip–substrate equilibrated configuration shown in Fig. 2(d) and

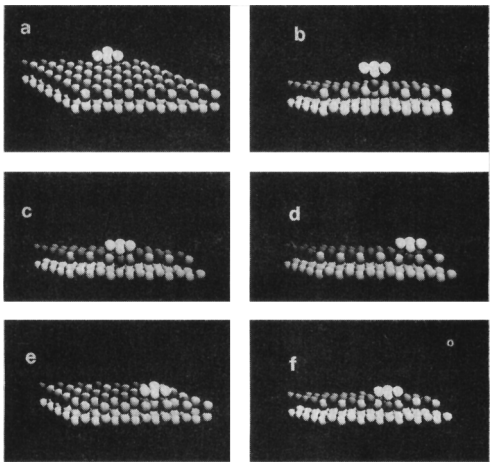

FIG. 2. Snapshots of small static tip–substrate atomic configurations. Tip atoms in bright white and topmost substrate layer as dark spheres. (a) Tip outside range of interaction; (b) tip lowered towards the surface, "lifting" the atom underneath it; (c) tip equilibrated with the surface at the lowered position (1.227 Å from the nominal position of the surface plane), demonstrating the formation of an interstitial defect under the tip (note location of the dark ball directly under the tip); (d) initial cofiguration before scan (translation of the tip to the left) begins; (e) configuration when the tip scans between substrate atoms; (f) configuration when the tip translated by one unit cell distance, inducing a new interstitial surface defect. The previous tip-induced interstitial [see (d)] returns to his original location in the first atomic layer.

moving the tip laterally to the left) show that when in the region between atoms the tip-induced interstitial returns to his original location in the first atomic layer [see Fig. 2(e)] and a new interstitial defect is generated when the tip moves to a location over the next atom in the surface row [Fig. 2(f)].

The consequences of the interaction between a large dynamic tip consisting of 102 atoms, arranged in four layers and exposing a 16-atom (111) facet, are exhibited in Fig. 3 where snapshots of the system configurations initially [Fig. 3(a)], at the lowered tip configuration [Fig. 3(b)], and after raising the tip [Fig. 3(c)], are shown. As seen, for this reactive system, lifting of the tip results in the formation of a "connective neck" consisting mostly of tip atoms. The variations in the normal component of the force on the tip atoms F_z, potential energy of the tip atom E_P, and their kinetic temperature T, are shown in Fig. 4(b)–4(d), respectively, as well as the temperature of the dynamic substrate and height of the tip assembly from the surface in Figs. (4e) and 4(a), respectively. The snapshots in Fig. 3(a)–3(c) correspond to times $t = 0$, 50, and 120 in Fig. 4. As seen from Fig. 4(b) at the equilibrium configuration, with the tip resting in contact with the surface, the total normal component of the force on the tip atoms is attractive ($F_z < 0$ in the time interval, $20 < t < 60$ tu). Subsequent raising of the tip ($t > 60$) results in an increased attraction between the tip and the substrate atoms and an increase in the potential energy [see Fig. 4(c)] of the tip atoms as the initial crystalline structure of the tip is modified due to strained bonding to the substrate. Further raising of the tip ($t \sim 100$) results in disruption of some of the bonds between the tip and substrate atoms, resulting in a sudden decrease in the force between them [see Fig. 4(b)],

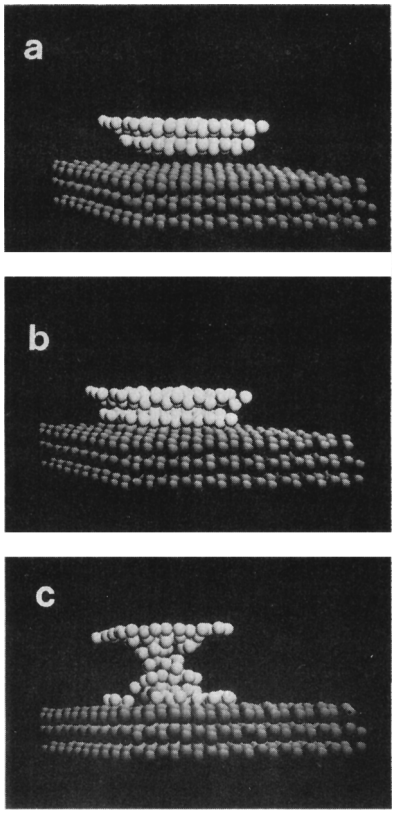

FIG. 3. Atomic configurations as a large faceted dynamical tip initially equilibrated outside the range of interaction (a), is lowered to a distance of 2.91 Å from the surface (b), and following equilibration is raised (c).

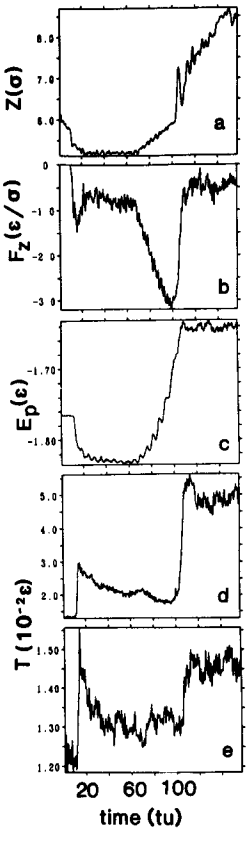

FIG. 4. Variation vs time (in tu $= 7.6634 \times 10^{-14}$ s) of: (a) Center of mass height of the tip-holder assembly, Z; (b) normal force on the tip, F_z (in units of $\epsilon/\sigma = 1.6572 \times 10^{-9}$ N; (c) potential energy of the tip atoms, E_p; (d) temperature of the tip atoms, (e) kinetic temperature of the dynamic substrate. Simulations are for lowering and raising of a large (102 atom) faceted ordered dynamical tip. See corresponding atomic configurations in Fig. 3.

an increase in the potential energy and a sudden rise in the tip and local substrate temperature [see Figs. 4(d) and 4(e)], yielding eventually the atomic configuration shown in Fig. 3(c).

In constant-force scanning simulations, in addition to the particle equations of motion, the center of mass of the tip-holder assembly, Z, is required to obey $M\ddot{Z} = (\vec{F}(t) - \vec{F}_{ext})\cdot\hat{Z} - \gamma\dot{Z}$ where $\vec{F}$ is the total force exerted by the tip-atoms on the static holder at time t, which corresponds to the force acting on the tip atoms due to their interaction with the substrate, $\vec{F}_{ext}$ is the desired (prescribed) force for a given scan, γ is a damping factor, and M is the mass of the holder. In these simulations the system is brought to equilibrium for a prescribed value of $F_{z,ext}$, and the scan proceeds as described above while the height of the tip-holder assembly adjusts dynamically according to the above feedback mechanism.

In Figs. 5(a)–5(d) and Fig. 6 we show the results for a constant-force scan, for $F_{z,ext} = -13\ \epsilon/\sigma$ (corresponding to -2.15×10^{-8} N, i.e., negative load). In these simulations the substrate consists of six dynamic layers with 100 atoms per layer. Side views of the system trajectories at the beginning and end stages of the scan are shown in Figs. 5(a) and 5(b), and 5(c), respectively. As seen, the tip–substrate interactions induce local modifications of the substrate and tip structure, which are transient (compare the surface structure under the tip at the beginning of the scan [Fig. 5(a)], exhibiting outward atomic displacements of the top-layer atoms, to that at the end of the scan [Fig. 5(c), where that region relaxed to the unperturbed configuration]. The recorded force on the tip holder along the scan direction (x)

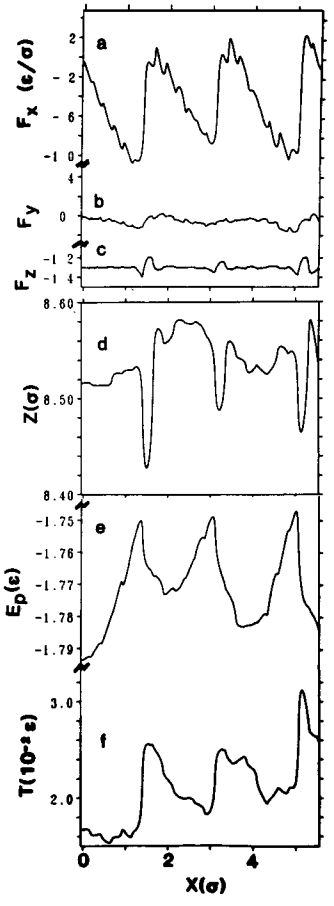

FIG. 6. Constant-force scan simulation at $F_{z,ext} = -13$ (i.e., negative load of -2.15×10^{-8} N), employing a large (102 atoms) faceted, ordered dynamical tip. (a)–(c) Variations of the force F_x (along the scan direction) and of the force components normal to it, F_y and F_z. Forces in the units of 1.6572×10^{-9} N. Note that the recorded force in the z direction fluctuates around the prescribed value; (d) center-of-mass height of the tip-holder assembly; (e) potential energy E_p of the tip atoms: (f) kinetic temperature of the tip atoms. Note the discontinuous variation and asymmetry in F_x, signifying stick–slip behavior, and the accompanying variations in E_p and T.

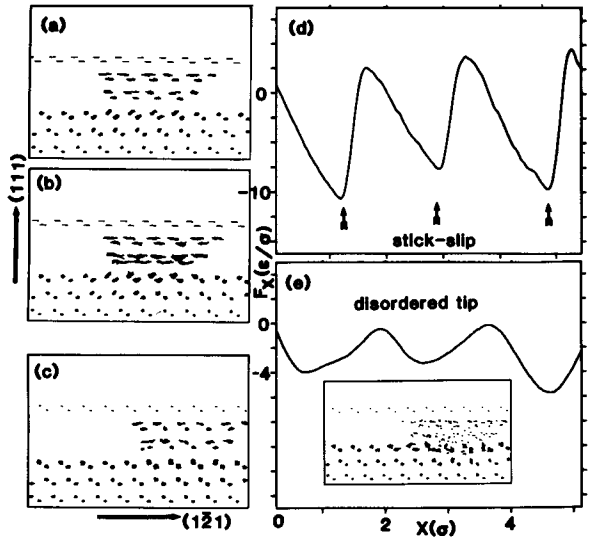

FIG. 5. (a)–(c) Particle trajectories in a constant-force simulation, $F_{z,ext} = -13.0$ (i.e., -2.15×10^{-8} N), viewed along the $(10\bar{1})$ direction just before (a) and after (b) a stick–slip event and towards the end of the scan (c), for a large, initially ordered, dynamic tip. (d) The recorded F_x, exhibiting stick–slip behavior. (e) The F_x force in a constant-force scan ($F_{z,ext} = 1.0$) employing a glassy static tip, exhibiting the periodicity of the substrate. Shown in the inset are the real-space trajectories towards the end of the scan, demonstrating the tip-induced substrate local modifications.

is shown in Fig. 5(d) and in Fig. 6(a), exhibiting a periodic modulation, portraying the periodicity of the substrate. At the same time the normal force F_z fluctuates around the prescribed value [Fig. 6(c)] and no significant variations are observed in the force component normal to the scan direction [F_y in Fig. 6(b)].

Most significant is the stick–slip behavior signified by the asymmetry in F_x [observed also in the real-space atomic trajectories in Figs. 5(a) and 5(b)]. Here, the tip atoms closest to the substrate attempt to remain in a favorable bonding environment as the tip-holder assembly proceeds to scan. When the forces on these atoms due to the other tip atoms exceed the forces from the substrate, they move rapidly by breaking their current bonds to the surface and forming new bonds in a region translated by one unit cell along the scan direction. The detailed energetics of the atomic-scale stick–slip phenomenon can be elucidated from the variations in the potential and kinetic energies of the tip atoms along the scan, shown in Fig. 6(e) and 6(f), respectively. As seen, during the stick stage, the potential energy of the strained bonds between the tip and substrate atoms increases. The slip stage is signified by a discontinuity in the force along the scan direction [F_x, in Fig. 6(a)], and by a sharp decrease in the potential energy [Fig. 6(e)], which is accompanied by a sudden increase in the kinetic temperature of the tip atoms [Fig. 6(f)] as a result of the disruption of the bonds to the substrate and rapid motion of the tip atoms to the new equilibrium positions. We note that the excess kinetic energy

(local heating) acquired by the tip during the rapid slip, dissipates effectively during the subsequent stick stage, via the tip to substrate interaction [see the gradual decrease in T in Fig. 6(f), following the sudden increase].

We note that our constant-force simulation method corresponds to the experiments in Ref. 7 in the limit of a stiff wire (lever) and thus the stick–slip phenomena which we observed are a direct consequence of the interplay between the surface forces between the tip and substrate atoms and the interatomic interactions in the tip. The F_x force which we record corresponds to the frictional force. From the extrema in F_x [Figs. 5(d) or 6(a)] and the load ($F_{z,\mathrm{ext}}$) used we obtain a coefficient of friction $\mu = |F_x|/|F_{z,\mathrm{ext}}| = 0.77$, in the range of typical values obtained from tribological measurements in vacuum, although we should caution against taking this comparison rigorously.

Results for a constant-force scan at a positive load ($F_{z,\mathrm{ext}} = 0.1$, i.e., 1.66×10^{-10} N), employing the large faceted tip, are shown in Fig. 7. As seen from Fig. 7(d), the center-of-mass height of the tip and holder assembly from the surface, Z, exhibits an almost monotonic decrease during the scan, in order to keep the force on the tip atoms around the prescribed value of 0.1 [see Fig. 7(e)]. At the same time the potential energy of the tip increases. This curious behavior corresponds to a "smearing" of the tip as revealed from the real-space trajectories shown in Figs. 7(a)–7(c). Comparison of the atomic configurations at the beginning [Fig. 7(a)], during the scan [Fig. 7(b) corresponding to $X\sim1\sigma$, demonstrating a slip] and towards the end of the scan [Fig. 7(c)] shows that as a result of the interactions between the tip and substrate atoms, the bottom layer of the tip adheres to the substrate and thus in order to maintain the same force on the tip holder throughout the scan (as required in the constant-force scan mode) the tip assembly must move closer to the substrate. These simulations demonstrate that in reactive tip–substrate systems, even under relatively small loads, rather drastic structural modifications may occur, such as "coating" of the substrate by the tip (or vice versa).

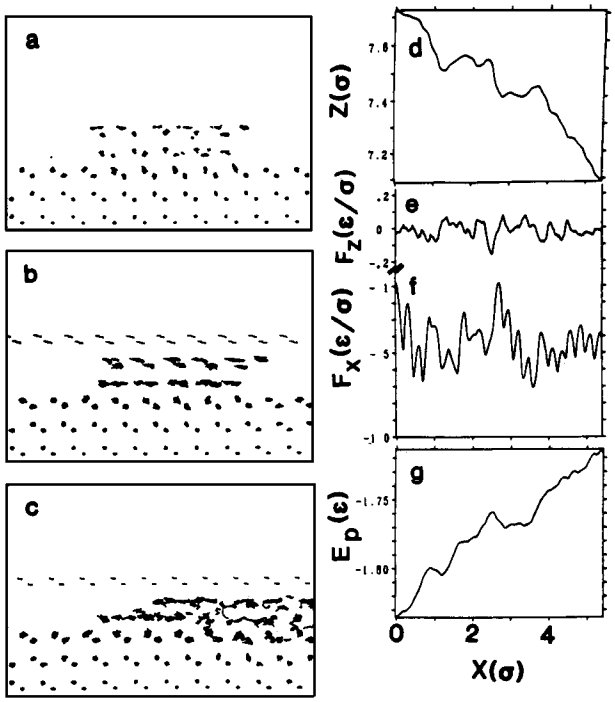

FIG. 7. Constant scan similation at $F_{z,\mathrm{ext}} = 0.1$ (i.e., 1.6572×10^{-10} N), employing a large (102 atoms), initially, ordered dynamic tip. (a)–(c) Real-space particle trajectories at selected times during the scan, beginning (a), middle (b), and end (c), respectively. Note that the bottom layer of the tip adheres to the substrate surface (c); (d) Center-of-mass height of the tip-holder assembly during the scan, as a function of scan distance, $\sigma = 2.0951$ Å. Note the decrease in height associated with the adherance of the bottom tip atoms to the substrate [see (c)]. (e), (f) Normal force F_z and tangential force in the direction of the scan F_x during the scan. (g) Potential energy of the tip atoms E_p during the scan.

The frictional force obtained in simulations employing a disordered rigid 102-atom tip, prepared by quenching of a molten droplet, scanning under a load $F_{z,\mathrm{ext}} = 1.0$ are shown in Fig. 5(e). The significance of this result lies in the periodic variation of the force, reflecting the atomic structure of the substrate. This demonstrates that microscopic investigations of structural characteristics and tribological properties of crystalline substrates are not limited to ordered tips.[7]

Finally, we note two most recent studies of tip–substrate interactions involving other materials. Employing an empirically constructed graphite potential and a potential for diamond[24] (both based on a reparametrization of the SW potentials, and in the case of graphite augmented by interlayer Lennard–Jones interactions), it was shown[24a] that for forces stated in the experimental literature, a monoatomic tip would cause very large relaxations of the graphite substrate extending over a large spatial extent,[8] with an eventual penetration of the surface at $\sim5\times10^{-8}$ N. Furthermore, it was shown that by assuming that the AFM tip carries a graphite flake, a wide variety of images seen by the atomic force microscope can be reproduced and correlated with relative rotations of the flake with respect to the scanned substrate. In other studies,[25] employing the embedded atom method (EAM), interactions between metal tips and metal substrates have been investigated. These studies demonstrate that as a consequence of the metallic cohesion, metallic tips lowered onto metallic substrates adhere to the substrate ("pressure welding") resulting in plastic deformation upon separation signified by a pronounced hysterises in the force versus distance records (upon loading and unloading), similar to the observations in recent AFM experiments.[26]

III. DYNAMICS OF BOUNDED THIN LIQUID FILMS

Studies of nonequilibrium systems, flow in particular, present immense theoretical and technical challenges. Coupled with the basic conceptual problems presented by nonequilibrium phenomena is the technological motivation related to the molecular design of fluids of desired rheological[27] and hydrodynamical characteristics for lubrication purposes. Lubricating fluids are made usually of polymeric molecules (sometime in colloidal suspension) which are characterized by structural and shear-stress relaxation times ranging from milliseconds to minutes, and the relevant flow rates are of the order of the reciprocal of these times. Thus, the Weissenburg number[27] for these materials (the product of shear rate and relaxation time) is of the order of

unity. While simulations of phenomena on the above time scales are computationally prohibitive, it is possible to study the nature of the rheological processes occurring in these systems via simulations of simpler fluids sheared at the same Weissenburg number.[28] Simple Lennard–Jones systems exhibit such "corresponding state" behavior.

To investigate the nature and properties of bounded thin fluid films at equilibrium and under shear, we have conducted systematic MD simulations of such systems under various external conditions and for a variety of interaction parameters. We demonstrate our results for a system composed of: (i) two fcc solid slabs each consisting of three dynamic and three static layers (with 70 particles/layer) exposing the (111) surface with the particles interacting via a 6–12 Lennard–Jones (LJ) potential [see Eq. (1), Sec. IV]. While periodic boundary conditions are imposed in directions parallel to the surface plane the system (dynamic solids and confined fluid) thickness in the [111] direction evolves dynamically under a load of $0.25\,\epsilon_{ss}/\sigma_{ss}^3$ (where ϵ_{ss} and σ_{ss} are the LJ parameters for the intersolid interactions), and (ii) 150 fluid particles of equal size, bounded between the dynamic solid interfaces, and interacting between themselves via a LJ potential with a well depth parameter $\epsilon_{ll} = \epsilon_{ss}/10$, and with the solid by $\epsilon_{ls} = (\epsilon_{ss}\epsilon_{ll})^{1/2}$. The temperature of the system is controlled at $T = 0.074$ (in reduced LJ units, i.e., ϵ_{ss}), slightly above the melting temperature of the fluid, via scaling of particles' velocities in the two dynamic layers which are not in direct contact with the liquid in each of the bounding solid slabs, which thus serve as a heat bath (i.e., particles in the solid layers at the interface and the fluid particles evolve freely with no temperature control, transferring heat to the substrate slab in a natural manner).

The density profile in the direction normal to the interface ([111], Z direction) at equilibrium ($T = 0.074$) is shown in Fig. 8(b) exhibiting layering in the fluid,[29] and short-time real-space trajectories of the solid and fluid layers at the interface exhibiting intralayer order and interlayer registry are shown in Fig. 9(a). The slab thickness (in units of $7\sigma_{ss}$) vs time (in reduced LJ time units, tu) is shown in Fig. 8(a) with the end of the equilibrium simulation corresponding to $t < 75$. At time $t = 75$ we apply a sudden shear velocity of 0.1 σ_{ss}/tu along the $[1,\bar{1},0]$ (x) direction to the static portions of the solid slabs (which as a result start translating in opposite directions since the velocities are applied to the opposing solid slabs in opposite senses). As seen from Fig. 8(a), upon application of the shear perturbation, the thickness of the system initially increases slightly (in major part in the fluid region which is set in motion in response to the shear perturbation) followed first by a steady decrease and subsequently by an abrupt drop (at $t \simeq 165$). Inspection of the density profiles at an intermediate time $\sim t = 160$ [Fig. 8(c)] and after steady-state is achieved [$t \simeq 210$, Fig. 8(d)] reveals that the change in the fluid film thickness is due to a collapse of the system from three to two fluid layers, which corresponds to an increase in areal density of the fluid layers by $\sim 20\%$. The pronounced intralayer structure of the fluid during steady-state shear is shown in Fig. 9(b). Accompanying this structural transition in the fluid is a marked increase in the peak-to-peak fluctuations of the internal shear stress (σ_{xz}) of the system (calculated from the instantaneous trajectories) as seen in Fig. 8(e). The very regular fluctuations in thickness (after collapse) seen in Fig. 8(a) coincide in frequency, with the passing of $(1,\bar{1},0)$ rows in the

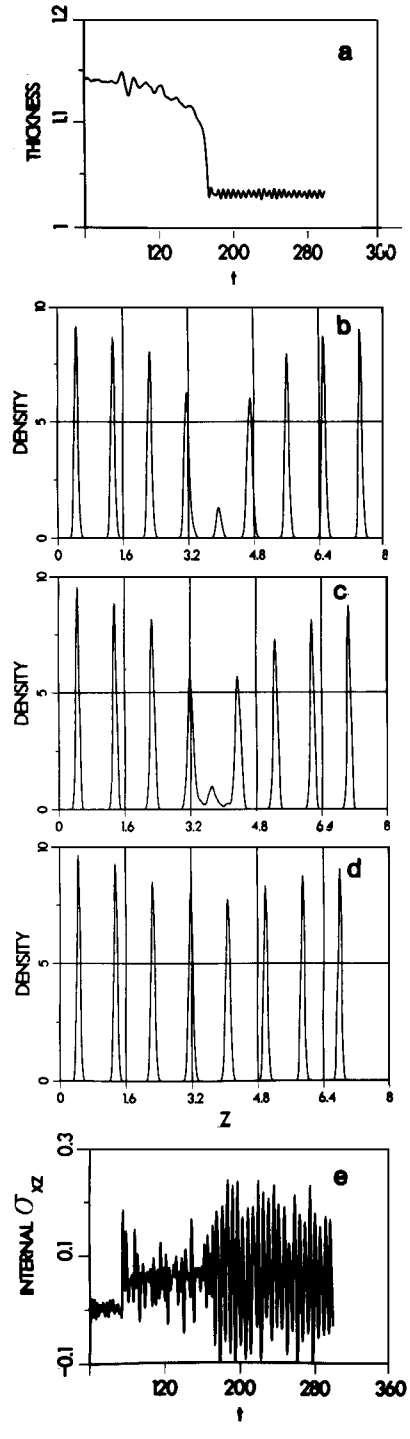

FIG. 8. Results of MD simulations of a fluid confined between parallel solid regions. (a) System thickness (in units of $7\sigma_{ss}$) vs time [in LJ tu]. For $t < 70$ system at equilibrium at $T = 0.074\,\epsilon_{ss}$. For $t > 75$ system under shear. (b) Density profile in the z ([111]) direction of the sheared system at $t = 130$ showing three dynamic solid layers on each side of a layered fluid (middle three layers). The middle fluid layer contains ~ 20 particles. (c) Same as (b) but under shear at $t = 160$ [see (a)]. (d) Same as (a) but at steady state under shear ($t = 210$) exhibiting the transition to a two-layer, structured fluid. z distance in (b)–(d) in units of σ_{ss}. (e) Internal shear stress (σ_{xz}, in units of $\epsilon_{ss}/\sigma_{ss}^3$) in the system vs time exhibiting an increase in peak-to-peak fluctuation upon the structural transition in the fluid.

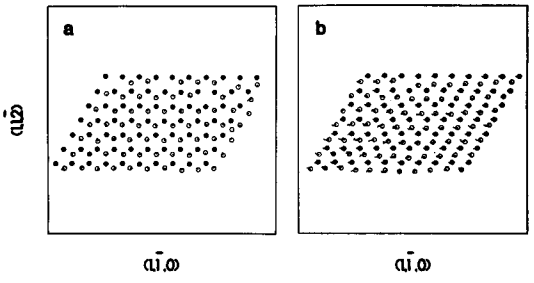

FIG. 9. (a) Short-time real-space trajectories of particles in the interfacial dynamic solid (filled circles) and fluid (empty circles) layers, exhibiting intralayer order and interlayer registry at equilibrium. (b) Same as (a) at steady state under shear. Note that the fluid layer under these conditions is denser than at equilibrium [compare to (a)]. The positions of the atoms at the start of the short-time interval are in the middle of the circles.

slip plane, indicating persistant order on both sides of the slip plane. These phenomena have similar characteristics to those observed recently by Israelachvili using an extension of the surface force apparatus,[3] indicating a structural dynamical mechanism which (in addition to film drainage) can be operative in such systems. We should note that for the above shear velocity the collapse of the film does not occur for a fluid film consisting of 160 particles. The properties and response of the system (including film drainage) for various film thicknesses, loads and shear velocities are under investigation. Finally, we note that in simulations of thick fluid films (e.g., three times thicker than in the above example), under low shear rates we have found[17] similar interfacial layering (involving 2–3 fluid layers) which decays into the middle of the fluid film, with the latter region exhibiting properties (viscosity and structure) similar to a bulk fluid under similar conditions. However, at higher shear rates the interfacial liquid-layering is much less pronounced and in addition non-Newtonian flow occurs.

Finally, recent theoretical studies in our laboratory[30a] have shown evidence for shear-induced ordering in atomic and molecular liquids which have been subsequently observed using the surface force apparatus.[30b]

These results and studies of the dependencies of the flow characteristics on the strength of the fluid–solid interaction and the composition and complexity of the fluid demonstrate the potential utility of MD simulations in tribological molecular design problems.

IV. DYNAMICAL SIMULATIONS OF STRESS, STRAIN AND FINITE DEFORMATIONS

Common observations related to tribological phenomena, and of thermomechanical properties and response of materials in general, are usually made at the continuum level.[31] Consequently, (and naturally) the development of theoretical understanding of these phenomena followed the "continuum modelling" approach.[31] The methodology of the development of these models is based on the principles of mass, momentum and energy balance, and the formulation of constitutive equations. While the mathematical formulation of classical models of the mechanical response of matter (such as the classical theories of elasticity and hydrodynamics) achieved a high degree of sophistication, current focus is on the incorporation of knowledge about the microscopic behavior of materials in continuum models which attempt to describe macroscopic observations. This is done via the introduction, into the continuum models, of a set of state variables which provide averaged (coarsened) representations of the relevant microscopic quantities. In addition we should note that most applied models of mechanical response are limited to the elastic (small spatial deformation) and linear (small rates of application of the external perturbation) regimes. Attempts to incorporate inelastic response and nonlinear effects result in a great (often prohibitive) complexity.

To gain knowledge about the energetics and atomic scale mechanisms and to identify and determine characteristic material and ambient parameters which underlie and govern the properties and response of materials requires experimental and theoretical methods which probe physical systems with refined spatial and temporal resolution. As we discussed above molecular dynamics (MD) simulations afford such investigations.

Traditionally, MD simulations have been employed in studies of systems of fixed shape and size of the periodically replicated calculational cell (i.e., constant volume simulations). More recently, methods for simulating systems in which the volume and shape of the calculational cell may vary dynamically have been developed,[32–38] opening the way to investigations of a large number of materials phenomena in which the dynamical freedom of the system to change volume and/or structure (or phase) is essential. In addition, a number of methods have been developed for simulations of flow and hydrodynamical systems[39–42] which allow detailed investigations of these nonequilibrium phenomena. Using molecular dynamics techniques various studies of the mechanical properties of solids and fluids have been reported. Among the investigations of solid systems we note studies of stressed solids and crack propagation,[43–48] dislocation energetics and dynamics,[46] structural transformations in crystal lattices under uniaxial tension or compression,[33,37,49,50] sliding and migration of grain boundaries,[37] simulations of plastic deformations[38] and shock wave dynamics,[51,52] studies of stressed interfaces,[38,40] and calculations of elastic coefficients using MD simulations.[53]

We have investigated[38,40] using MD simulations the microscopic dynamical response, deformation, and stress relief mechanisms at crystalline solid interfaces subject to externally applied perturbations. (Constant thermodynamic tension, constant strain-rate and isoexternal-stress simulations have been performed.) The objectives of these studies were: (i) identification of the mechanisms for solid interfacial systems of deformation, stress accumulation and relief and the dynamical response to external perturbations, (ii) identification of the dependence of the above phenomena on material characteristics, such as bonding strength, atomic sizes and interface crystallography and on ambient conditions (thermally adiabatic versus isothermal), and (iii) the development and critical assessment of MD simulation methods for investigations of the above phenomena.

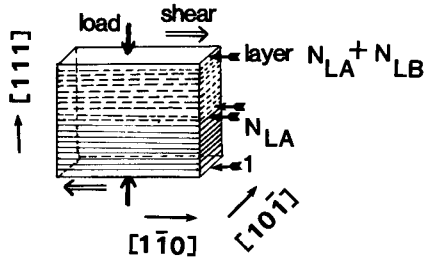

FIG. 10. A schematic of the calculational cell. N_{LA} is the number of layers in the A (hard) material and N_{LB} the number of layers in the B (soft) material. The interface is between layers N_{LA} and $N_{LA}+1$. The direction of the applied load and shear stresses are indicated. Three-dimensional periodic boundary conditions are employed in the simulations.

In these studies we focus on the mechanisms and dynamics of the response of a system containing an interface between two materials to external stresses. The model system which we employ in our simulations consists of N particles (N_A of type A and N_B of type B, $N_A+N_B=N$) interacting via pairwise 6–12 Lennard-Jones (LJ) potentials:

$$V(r)=4\epsilon_{\alpha\beta}\left[\left[\frac{\sigma_{\alpha\beta}}{r}\right]^{12}-\left[\frac{\sigma_{\alpha\beta}}{r}\right]^{6}\right],(\alpha,\beta)=A,B, \quad (1)$$

where A and B represent two types of materials. The solid is set up initially in a fcc crystalline structure, with N_L (111) layers (N/N_L particles per layer) with the Z axis along the [111] direction,[54] and three-dimensional periodic boundary conditions are used (see Fig. 10). The well-depth parameter ($\epsilon_{\alpha\beta}$) of the interaction potential between particles in layers 1 through N_{LA} is taken to be twice that for particles in layers $N_{LA}+1$ through N (i.e., $\epsilon_{AA}=2\epsilon_{BB}$) corresponding to a soft, solid, lubricating material (the B system) pressed between hard-material slabs (the A system). In order to isolate the dependence of the system response on the interaction strength (potential depth) parameter ϵ from that due to differences in the atomic sizes (and thus interatomic distances) associated with the parameter σ in the LJ potential, we have performed first simulations in which $\epsilon_{AA}=2\epsilon_{BB}$ and $\sigma_{AA}=\sigma_{BB}$, and then simulations in which $\sigma_{BB}=1.5\sigma_{AA}$. The interspecies LJ potential parameters were chosen as $\sigma_{AB}=(\sigma_{AA}+\sigma_{BB})/2$ and $\epsilon_{AB}=(\epsilon_{AA}\epsilon_{BB})^{1/2}$. In the following we use reduced units[55] where energy and temperature are expressed in units of ϵ_{AA}, length in units of σ_{AA}, stress in units of $(\epsilon_{AA}/\sigma_{AA}^3)$ and the time unit (tu) is $(m_A/\epsilon_{AA})^{1/2}\sigma_{AA}$. In the integration of the equations of motion we used a time step $\Delta t=0.0075$ tu which results in energy conservation (to six significant figures) for extended runs.

Following equilibration of the initial system at a reduced temperature of $T=0.11$ (note that a pure bulk LJ crystal melts at $T\simeq 0.7$, and thus, since $\epsilon_{BB}=\epsilon_{AA}/2$, the bulk melting point of the soft material B is half that of the A material) under a load of 0.5 in the [111] (Z) direction we apply the external perturbation. In simulations of applied thermodynamic tension [isoenthalpic, isotension and constant number of particle, N, simulations, i.e., the ($\mathscr{H},\tau,N$) ensemble] we apply to the system a thermodynamic tension tensor τ (which is related to the external stress tensor) in the [1,$\bar{1}$,0] direction (see Fig. 10) at a rate of $\dot{\tau}_{xz}=0.00125\ (\epsilon/\sigma^3)/\Delta t$ and follow the evolution of the system until it fails [to keep the system from a rigid rotation a symmetric thermodynamic tension tensor τ is applied, (i.e., $\tau_{xz}=\tau_{zx}$)].

To investigate the dependence on the thermal ambient conditions we distinguish between simulations where the system is thermally isolated during the application of the shear and simulations where isothermal conditions are maintained. As the system envolves under the applied shear it develops internal stresses which are calculated using the positions and forces on the particles.[38] These simulations allow us to determine the nature of structural transformations and the critical external stresses (or critical strains in constant strain-rate simulations) which characterize the transition from elastic to inelastic response regimes, and the critical yield stress (where the internal stresses vanish).

The mechanical response and energetic characteristics of the system can be investigated via layer decomposition of the system properties. Results at a constant external $\tau_{s,xz}=0.81$ and adiabatic thermal conditions for a system composed of nine layers each of equal size particles of hard and soft materials (with 70 particles/layer and the interface located between layers 9 and 10), which exhibited yield at a critical value of $\tau_{c,xz}=0.86$, are shown in Figs. 11 and 12. Inspection of the real space trajectories revealed that at this value of stress (which is below the critical yield value) the system undergoes a structural transformation involving interlayer motion leading to stacking fault generation (between layers 12 and 13) inside the soft material and slip.

In Fig. 11(a) and 11(b) we depict the per layer xz component of the internal stress for the interface layers (layer 5, 8, and 9 of the hard material and layers 10–14 of the soft mate-

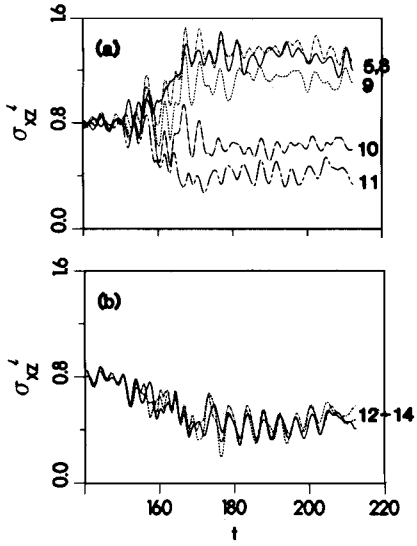

FIG. 11. Per-layer internal stresses (σ^l_{xz}) vs time (in tu) for a simulation at $\tau_{xz}=0.81$ under adiabatic conditions. Layers 5, 8, and 9 in the hard materials and 10 and 11 in the soft ones are shown in (a). The stresses in layers 12–14 in the soft material are shown in (b). The interface is between layers 9 and 10. Note the variation in the internal stresses at the time of the structural transformation. The internal stresses in the interior of the soft material (10–14) decrease with layer 10 exhibiting pinning by the hard material. The stress relief in the soft material is accompanied by stress accumulation in the hard material (layers 5–9).

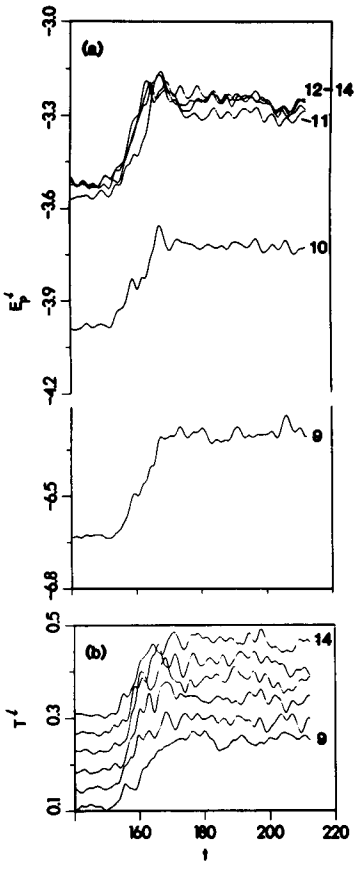

FIG. 12. Per layer potential energies, E_p^l in (a), and temperatures T^l in (b), for the system simulated at $\tau_{xz} = 0.81$ under adiabatic conditions.

rial). From these figures we observe that the generation of the structural transition involves a gradual decrease in the internal σ_{xz} component in layers 11–14 of the soft material while the variation in the stress in layer 10 [the atomic plane of the soft material (B) adjacent to the hard material (A), see Fig. 10] is smaller. As seen from Fig. 11(a) the *stress relief* process and the associated structural transformation in the *soft material* are accompanied by a *stress accumulation in the interfacial region of the hard material* (layer 9). In addition we observe periodic oscillations in the internal stress (most pronounced for layers 11–14) past the structural transformation period, as the system relaxes in the new state after the structural transformation events.

The energetics of the system is explored via the time records of the perlayer potential energies (E_p^l) and temperature (T^l) shown in Figs. 12(a) and 12(b), respectively. From the potential energy curves we find that the potential energy of particles in layer 11 (second layer from the interface, see Fig. 10) in the soft material is initially lower than that of layers 12–14, which are further removed from the interface, since particles in that layer are within the range of the stronger interaction with the hard substrate $[\epsilon_{AB} = \epsilon_{AA}\epsilon_{BB})^{1/2}]$. The potential energy of particles in the interfacial soft material layer (layer 10) adjacent to the hard material is lower by about $-0.4\,\epsilon$ than the value for layer 11. This extra stabilization "pins" this interfacial layer to the hard substrate. The potential energy of the topmost layer of the hard material (layer 9) is lower further by about -2.6ϵ. The potential energies of both layers 9 and 10 increase due to the structural transformation. Since the system in this set of calculations is thermally isolated, the structural change is accompanied by a temperature increase as seen from Fig. 12(b) (where the curves for successive layers, starting from 10 and up, are displaced vertically by 0.04ϵ). Note however that the final temperature after the transformation is below the melting temperature for both materials.

To investigate the dependence of the system properties on the mismatch in atomic sizes between the two interfacing materials, we have performed simulations in which the well-depth parameters were chosen as before but the σ parameters were chosen such that the atoms in the soft (B) material are characterized as having a larger size, i.e., $\sigma_{BB} = 1.5\,\sigma_{AA}$ and $\sigma_{AB} = 1.25\,\sigma_{AA}$. From these simulations we have determined that the critical yield value of the thermodynamic tension in this system is $\tau_{c,xz} = 0.62 \pm 0.01$ (and the corresponding external stress $\sigma_{ec,xz} = 0.51 \pm 0.01$), which are considerably lower than the corresponding values found for the equal-atomic size systems. Moreover, unlike the previous cases, where yield was preceded by an external stress regime in which the system responded inelastically via a sequence of structural transformations, for the present system (in which the atomic sizes across the interface differ) no such behavior is observed. Furthermore, the whole soft system responds in unison, starting at the interfacial layer and up into the material. These observations can be understood when considering that as a consequence of the larger atomic size the atoms of the soft material at the interface average over the corrugation of the potential due to the substrate, resulting in an effective potential surface which exhibits smaller variations for lateral displacements parallel to the interface plane, and consequently a reduced resistance to shear.

The results of our extensive investigations[38] may be summarized as follows: (i) For interfacial systems which are characterized by differing interatomic interaction strengths (i.e., the interface is between a hard and soft material), the system responds to an applied nonisotropic perturbation (applied shear or strain) first elastically and then via stress relief mechanisms which involve structural transformations (stacking fault formation and interlayer slip). For larger values of the external forces, eventual yield occurs. (ii) Critical values of the external perturbation required in order to bring about inelastic response (structural transformations and yield) have been determined. Our simulations demonstrate that the critical values are smaller for a system under thermally adiabatic conditions than for an isothermal environment. The origin of the difference lies in the dissipation of the generated thermal energy under isothermal conditions, which necessitates larger values of the external perturbations in order to overcome potential barriers for structural modifications and eventual yield. (iii) The cohesive interatomic interactions at the interface between a hard substrate and a soft material result in "pinning" of the soft material at the interface (1–3 atomic layers). As a result the response of the system to the external perturbation (stress relief via plastic as well as structural transformations) occurs in a "shear band" consisting of a few atomic layers inside the soft material, which for our model system are located at about 1–3

layers away from the original (unstressed) interface. The stress relief in the soft material is accompanied by stress accumulation in the hard substrate. (iv) MD simulations for interfacing hard and soft materials, which in addition are characterized by differing atomic sizes, reveal the important role played by atomic size mismatch in determining the atomic-scale mechanism of response. For such system it was found that no adhesive "pinning" occurs at the interface, and that the soft (and larger atomic size) material responds as a whole with no distinct structural transformations preceding the yield point. The critical yield stress value for this system is significantly lower than that found for the corresponding equal-atomic-size system. (v) Comparison of our results in this study for the [111] interface with our previous investigations of the [100] interface[40] demonstrates the dependence of the critical values of the shear stresses on the crystallographic orientation of the interface, as well as of certain details of the stress relief mechanisms.

ACKNOWLEDGMENTS

These studies were supported by the U. S. DOE Grant No. FG05-86ER-45234, the DARPA-Hughes, Tribological Fundamentals Program and the NSF Tribology Program. Most of the simulations were performed on the CRAY-XMP at NMFECC, Livermore, California, the CDC CYBER-990 at the Georgia Institute of Technology and at the Pittsburgh supercomputer center.

[1]R. P.Feynman, in *Miniaturization*, edited by H. D. Gilbert (Reinhold, New York, 1961), p. 282.
[2]J. N. Israelachvili, Acc. Chem. Res. **20**, 415 (1987); Proc. Nat. Acad. Sci. U.S.A. **84**, 4722 (1987).
[3]J. N. Israelachvili, P. M. McGuiggan, and A. M. Homola, Science **240**, 189 (1988).
[4]G. Binnig, H. Rohrer, Ch. Gerber, and E. Weibel, Phys. Rev. Lett. **50**, 120 (1983); G. Binnig and H. Rohrer, IBM J. Res. Dev. **30**, 355 (1986).
[5]G. Binnig, C. F. Quate, and Ch. Gerber, Phys. Rev. Lett. **56**, 930 (1986).
[6]P. K. Hansma and J. Tersoff, J. Appl. Phys. **61**, R1 (1986); R. J. Colton and J. S. Murday ONR Review (in press).
[7]C. W. Mate, G. M. McClelland, R. Erlandsson, and S. Chiang, Phys. Rev. Lett. **59**, 1942 (1987).
[8]J. M. Soler, A. M. Baro, N. Garcia, and H. Rohrer, Phys. Rev. Lett. **57**, 444 (1986); see comment by J. B. Pethica, *ibid.* **57**, 3235 (1986).
[9]J. M. Gimzewski and R. Moller, Phys. Rev. B **36**, 1284 (1987).
[10]See articles in *Molecular Dynamics Simulations of Statistical-Mechanical Systems*, Fermi School, XCVII, Corso, Varenna, 1985, edited by G. Ciccotti and W. G. Hoover (Soc. Ital. di Fisica, Bologna, 1986).
[11]U. Landman, R. N. Barnett, C. L. Cleveland, W. D. Luedtke, M. W. Ribarsky, D. Scharf, and J. Jortner, in *Material Research Society Symposium Proceedings* (Materials Research Society, Boston, 1985), Vol. 63, p. 273.
[12]F. F. Abraham, Adv. Phys. **35**, 1 (1986); J. Vac. Sci. Technol. B **2**, 534 (1984).
[13]Mater. Res. Soc. Bull. XIII (2), 14 (1988).
[14]U. Landman, R. N. Barnett, C. L. Cleveland, J. Luo, D.Scharf, and J. Jortner, AIP Conf. Proc. **162**, 200 (1987).
[15]D. W. Heerman, *Computer Simulation Methods* (Springer, Berlin, 1986).
[16]*Computer Simulations of Solids*, edited by C. R. A. Catlow and W. C. Machord (Springer, Berlin, 1982).
[17]U. Landman, in *Computer Simulation Studies in Condensed Matter Physics: Recent Developments*, edited by D. P. Landau, K. K. Mon, and H.-B. Schuttler (Springer, Berlin, 1988).
[18]See U. Landman and W. D. Luedtke in *Atomistic Modeling in Materials: Beyond Pair-Potentials*, edited by V. Vitek (Plenum, New York, 1988).
[19]See U. Landman, D. W. Luedtke and M. W. Ribarsky, in *New Materials Approaches to Tribology: Theory and Applications*, edited by L. E. Pope, L. Fehrenbacher and W. O. Winer (Materials Research Society, Boston, 1989).
[20]F. H. Stillinger and T. A. Weber, Phys. Rev. B **31**, 5262 (1985).
[21]U. Landman, W. D. Luedtke, R. N. Barnett, C. L. Cleveland, M. W. Ribarsky *et al.*, Phys. Rev. Lett. **56**, 155 (1986); F. F. Abraham and J. Q. Broughton, *ibid.* **59**, 64 (1987); W. D. Luedtke and U. Landman, Phys. Rev. B **37**, 4656 (1988); U. Landman, W. D. Luedtke, M. W. Ribarsky, R. N. Barnett, and C. L. Cleveland, Phys. Rev. B **37**, 4637, 4647 (1988); F. F. Abraham and I. P. Batra, Surf. Sci. **163**, L752 (1985).
[22]F. F. Abraham, I. P. Batra, and S. Ciraci, Phys. Rev. Lett. **60**, 1314 (1988).
[23]U. Landman, W. D. Luedtke, and A. Nitzan, Surf. Sci. **210**, L177 (1989).
[24](a) F. F. Abraham and I. P. Batra, Surf. Sci. Lett. **209**, L125 (1989); (b) W. D. Luedtke and U. Landman (unpublished).
[25]W. D. Luedtke, U. Landman, and R . N. Barnett (to be published).
[26]N. A. Burnham, I. L. Singer, and R. J. Colton (private communication).
[27]H. A. Barnes, *Dispersion Rheology* (Royal Society of Chemistry, London, 1980).
[28]D. M. Heyes, Mol. Phys. **57**, 1265 (1986).
[29]For MD results and earlier references about layering of interfacial fluids see U. Landman, R. N. Barnett, C. L. Cleveland, and R. H. Rast, J. Vac. Sci. Technol. A **3**, 1574 (1985).
[30](a) M. W. Ribarsky, U. Landman, and W. D. Luedtke (to be published), reported at the 35th AVS National Symposium, October, 1988, Atlanta, Ga. (b) J. N. Israelachvili (private communication).
[31]See review on "Continuum Modeling" by L. Davison in Mat. Res. Soc. Bull. **8**, 14 (1988); see also *Approaches to Modeling of Friction and Wear*, edited by F. F. Ling and C. H. T. Pass (Springer, Berlin, 1988).
[32]H. C. Andersen, J. Chem. Phys. **72**, 2384 (1980).
[33]M. Parrinello and A. Rahman, J. Appl. Phys. **52**, 7182 (1981).
[34]J. R. Ray and A. Rahman, J. Chem. Phys. **80**, 4423 (1984).
[35]For an extension to metallic systems see R. N. Bartnett, C. L. Cleveland, and U. Landman, Phys. Rev. Lett. **54**, 1679 (1985); *ibid.* Phys. Rev. Lett. **55**, 2035 (1985).
[36]W. G. Hoover, Phys. Rev. A **118**, 111 (1983).
[37]See reviews by S. Yip and M. Parrinello in Ref. 10.
[38]M. W. Ribarsky and U. Landman, Phys. Rev. B **38**, 9522 (1988).
[39]See recent reviews by D. J. Evans and G. P. Morriss, Comput. Phys. Rep. **1**, 297 (1984), and D. J. Evans and W. G. Hoover, Ann. Rev. Fluid Mech. **18**, 243 (1986).
[40]M. W. Ribarsky and U. Landman in *Approaches to Modeling of Friction and Wear*, edited by F. F. Ling and C. H. T. Pan (Springer-Verlag, New York, 1988), p. 159.
[41]S. Sutton, M. W. Ribarsky, and U. Landman, J. Chem. Phys. (to be published).
[42]C. L. Cleveland, J. Chem. Phys. **89**, 4987 (1988).
[43]G. J. Dienes and A. Paskin, in *Atomistic of Fracture*, edited by R. M. Latanison and J. R. Pickens (Plenum, New York, 1983), p. 671; A. Paskin, K. Sieradzki, D. K. Som, and G. J. Dienes, Acta Metall. **31**, 1253 (1983).
[44]B. DeCelis, A. S. Argon, and S. Yip, J. Appl. Phys. **54**, 4864 (1983) and references therein.
[45]W. T. Ashurst and W. G. Hoover, Phys. Rev. B **14**, 1465 (1976).
[46]W. G. Hoover, N. E. Hoover, and W. C. Moss, J. Appl. Phys. **50**, 829 (1979); see also A. J. C. Ladd and W. G. Hoover, Phys. Rev. B **26**, 5469 (1982).
[47]P. C. Gehlan, G. T. Hahn, and M. F. Kanninen, Scr. Metall. **6**, 1087 (1972).
[48]See review by M. I. Baskas and M. S. Daw in *Computer Simulations in Materials Science*, edited by R. J. Arsenault, J. Beeler, and D. M. Esterling (American Society for Metals, Cleveland, 1988).
[49]R. Najafabadi and S. Yip, Scr. Metall. **17**, 1199 (1983).
[50]J. R. Ray and A. Rahman, J. Chem. Phys. **82**, 4243 (1985).
[51]B. Moran, A. J. C. Ladd, and W. G. Hoover, Phys. Rev. B **28**, 1756 (1983).
[52]B. L. Holian, Phys. Rev. A **37**, 2562 (1988).

[53]M. D. Kluge, J. R. Ray, and A. Rahman, J. Chem. Phys. **85**, 4028 (1986); M. D. Kluge and J. R. Ray, Phys. Rev. B **37**, 4132 (1988).

[54]This interface orientation was chosen in view of our previous studies of the [001] interface (see Ref. 40), where it was found that slip occurs for the Lennard–Jones fcc system along the (111) planes. Note that the values for external stress given in Ref. 40, should be interpreted as those for the thermodynamic tension.

[55]If the interaction parameters are chosen such that they correspond to the cohesive energy and lattice constant of nickel ($\epsilon = 3.54\times10^{-13}$ erg, $\sigma = 2.49$ Å, and atomic mass $m = 9.75\times10^{-23}$ g) a reduced temperature $T = 0.11$ corresponds to 300 K, the reduced melting temperature $T_m = 0.7$ corresponding to 2000 K, the reduced unit of stress or load to 2.4×10^{7} g/cm^2 (or 2.4×10^{10} dynes/cm^2), and the reduced time unit (tu) corresponds to 4.1×10^{-13} s.